Faraday patterns in coupled one-dimensional dipolar condensates

Kazimierz Łakomy,[1] Rejish Nath,[2] and Luis Santos[1]
[1]*Institut für Theoretische Physik, Leibniz Universität, Hannover, Appelstrasse 2, D-30167 Hannover, Germany*
[2]*IQOQI and Institute for Theoretical Physics, University of Innsbruck, A-6020 Innsbruck, Austria*
(Received 12 July 2012; published 17 August 2012)

We study Faraday patterns in quasi-one-dimensional dipolar Bose-Einstein condensates with parametrically driven dipolar interactions. We show that in the presence of a roton minimum in the excitation spectrum, the emergent Faraday waves differ substantially in two- and one-dimensional geometries, providing a clear example of the key role of confinement dimensionality in dipolar gases. Moreover, Faraday patterns constitute an excellent tool to study nonlocal effects in polar gases, as we illustrate with two parallel quasi-one-dimensional dipolar condensates. Nonlocal interactions between the condensates give rise to an excitation spectrum characterized by symmetric and antisymmetric modes, even in the absence of hopping. We show that this feature, absent in nondipolar gases, results in a critical driving frequency at which a marked transition occurs between correlated and anticorrelated Faraday patterns in the two condensates. Interestingly, at this critical frequency, the emergent Faraday pattern stems from a spontaneous symmetry-breaking mechanism.

DOI: 10.1103/PhysRevA.86.023620 PACS number(s): 03.75.Kk, 89.75.Kd, 05.30.Jp

I. INTRODUCTION

Interparticle interactions play an essential role in the physics of ultracold gases. Although in many experiments these interactions may be approximated by a contact potential, there is a rapidly growing interest in a novel type of cold gases in which electric or magnetic dipole-dipole interactions (DDI) are crucial for the occurring phenomena. These so-called dipolar gases include atoms with large magnetic moments [1–3], polar molecules [4–6], and Rydberg gases [7]. The distinct nature of the dipolar interactions leads to a wealth of novel physics, including a geometry-dependent stability and a rotonlike minimum in the excitation spectrum (for reviews, see, e.g., Refs. [8,9]).

Interestingly, the long-range dipolar interactions result in an inherent nonlocal nature of dipolar gases, particularly striking in deep optical lattices. For nondipolar systems, gases trapped in different sites of a deep lattice do not interact with each other. Hence, for a vanishing intersite hopping, different sites may be considered as independent, uncorrelated experiments. In contrast, intersite DDI play a substantial role even in the absence of hopping. Recent lattice experiments have shown that the intersite dipolar interactions are the key element in the dynamics [10], as well as in the stability and collapse of dipolar condensates [11,12].

Faraday patterns constitute a paradigmatic example of pattern formation in periodically driven systems [13,14], ranging from classical fluids [15] through multimode lasers [16] and superfluid helium [17]. Interestingly, Faraday patterns may be observed in Bose-Einstein condensates (BECs) by modulating the nonlinearity resulting from the interatomic interactions [18–23], as shown in recent experiments [24]. Faraday patterns in BECs may be directly linked to the spectrum of elementary excitations, and in this sense provide an excellent insight into the fundamental properties of the condensates. In nondipolar gases, the Faraday pattern selection is determined uniquely for each modulation frequency due to the monotonically growing character of the excitation energy [25]. Interestingly, this is no longer the case for dipolar BECs with a rotonlike minimum in the excitation spectrum [26]. As a result, it has been shown that Faraday patterns in two-dimensional (2D) dipolar condensates present remarkable qualitative novel features [27].

In this paper, we analyze quasi-one-dimensional (quasi-1D) dipolar condensates with periodically driven dipolar interactions. We demonstrate that Faraday patterns provide a clear example of the nontrivial role of confinement dimensionality in dipolar gases, showing that in the presence of a rotonlike minimum in the excitation spectrum, Faraday patterns in a quasi-1D trap differ significantly with respect to the 2D case [27]. Moreover, Faraday patterns provide an excellent tool for the study of nonlocal effects in dipolar condensates, as we illustrate with two parallel quasi-1D BECs, in the absence of tunneling. The nonlocal dipolar interactions between both BECs lead to an unfolding of the excitation spectrum into symmetric and antisymmetric modes with respect to the transposition of the two condensates. We show that, as a consequence, at a critical driving frequency, a transition between correlated (symmetric) and anticorrelated (antisymmetric) Faraday patterns in the two BECs occurs. For the critical driving, the emergent Faraday pattern differs from one realization to another, resulting from a spontaneous symmetry-breaking mechanism.

The paper is structured as follows. In Sec. II we introduce the model for periodically driven quasi-1D dipolar condensates. Section III is devoted to Faraday patterns in a single quasi-1D BEC, with a focus on the differences compared to 2D condensates. Section IV is dedicated to the effects of the intercondensate dipolar interactions on the Faraday pattern selection in two parallel disjoint quasi-1D dipolar condensates. We conclude in Sec. V.

II. MODEL

We consider in this paper quasi-1D dipolar BECs, either in a single trap (Sec. III) or in two parallel traps (Sec. IV). Since the former case may be considered as a particular realization of the latter, we present in this section the general formalism for parallel quasi-1D BECs aligned along the z axis, and separated along the y axis by a distance Δ. We assume that the potential barrier separating both quasi-1D BECs is sufficiently

large to suppress any hopping between them. Each condensate experiences a strong harmonic confinement of frequency $\omega_\perp$ in the x-y plane and no confinement along the z direction. The atoms possess a magnetic dipole moment μ (the results are equally valid for electric dipoles) oriented by an external field along the y axis. We employ dimensionless expressions, using units of frequency $\omega_\perp$ and length $l_\perp = \sqrt{\hbar/M\omega_\perp}$, with M being the particle mass.

Due to the strong x-y confinement, we assume that the system remains in the ground state of the x-y harmonic oscillator (this condition is self-consistently verified), and we employ the nonlocal nonlinear Schrödinger formalism developed in Refs. [28,29] for a stack of quasi-1D dipolar BECs to obtain the coupled equations for the wave functions $\psi_j(z)$ in traps $j = 1,2$:

$$i\partial_t\psi_j(z) = \Big[-\frac{1}{2}\partial_z^2 + gn_j(z) + \frac{2\pi}{3}g_d\sum_m\int dk_z e^{ik_z z}\hat{n}_m(k_z) \times F_{|m-j|}(k_z)\Big]\psi_j(z). \quad (1)$$

Short-range interactions are characterized by the coupling constant $g = g^{3D}n_0/2\pi\hbar\omega_\perp l_\perp^3$, where n_0 is the linear density, and $g^{3D} = 4\pi a_{sc}\hbar^2/M$, with a_{sc} as the s-wave scattering length. The DDI are determined by the coupling constant $g_d = g_d^{3D}n_0/2\pi\hbar\omega_\perp l_\perp^3$, where $g_d^{3D} = \mu_0\mu^2/4\pi$, with μ_0 as the vacuum permeability. In Eq. (1), $\hat{n}_m(k_z)$ is the Fourier transform of the linear density $n_m(z) = |\psi_m(z)|^2$, and

$$F_p(k_z) = \int_0^\infty dk\frac{ke^{-\frac{1}{2}k^2}}{k^2+k_z^2}\big[\big(k^2-2k_z^2\big)J_0(k\Delta p) - 3k^2J_2(k\Delta p)\big], \quad (2)$$

where $J_n(x)$ are the Bessel functions of the first kind.

In the following, we consider a parametric modulation of the dipole-dipole interactions,

$$g_d(t) = \overline{g}_d[1+2\alpha\cos(2\omega t)], \quad (3)$$

where α characterizes the modulation strength. Such modulation may be implemented with intensity oscillations of the polarizing electric field for the case of polar molecules, or with additional transverse magnetic fields, which lead to a precession of the dipole moment orientation, for the case of magnetic dipoles.

The modulation of g_d induces Faraday waves. With the aim of examining the growth of such patterns, we introduce the following ansatz for the wave functions:

$$\psi_j(z,t) = \psi_{j_H}[1+A_j(t)\cos(qz)], \quad (4)$$

which describes correctly the physics of the pattern in the linear regime, where the modulation is weak and we may consider each momentum component q of the pattern separately. In Eq. (4), we introduce the complex amplitude $A_j(t) = u_j(t) + iv_j(t)$, which determines the perturbation from the initial homogeneous solution $\psi_{j_H} = \exp\{-i\overline{\mu}_j[t + (\Omega_j/\omega)\sin(2\omega t)]\}$, where $\Omega_j = \alpha(1-\overline{g}_d/\overline{\mu}_j)$, and $\overline{\mu}_j = g + \frac{2\pi}{3}\overline{g}_d\sum F_{|m-j|}(0)$ is the chemical potential. By inserting Eqs. (3) and (4) into Eq. (1), and linearizing in A_j, we arrive at

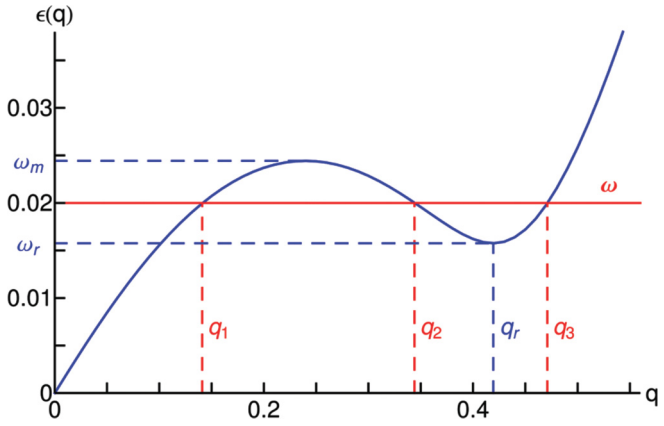

FIG. 1. (Color online) Excitation spectrum $\epsilon(q)$ of a single quasi-1D dipolar BEC, with $g = -0.1007$, $g_d = 0.0629$. Note the roton minimum at $\omega_r = \epsilon(q_r)$ and the maxon maximum at ω_m. For a driving frequency $\omega_r < \omega < \omega_m$, there are three possible momenta $q_{1,2,3}$ obeying the resonance condition $\omega = \epsilon(q)$.

the system of equations describing the modulation dynamics,

$$\frac{d^2u_j}{dt^2} + \frac{q^2}{2}\Big[\Big(\frac{q^2}{2}+2g\Big)u_j + \frac{4\pi}{3}g_d(t)\sum_m u_m F_{|m-j|}(q)\Big] = 0. \quad (5)$$

III. FARADAY PATTERNS IN A SINGLE QUASI-1D DIPOLAR BOSE-EINSTEIN CONDENSATE

We consider in this section the case of a single condensate, being particularly interested in the differences between the emergent Faraday patterns in a quasi-1D trap and those predicted in Ref. [27] for a 2D condensate. Employing a similar Bogoliubov analysis as the one presented in Ref. [28], we obtain the spectrum of elementary excitations in the considered case (see Fig. 1):

$$\epsilon(q) = \sqrt{\frac{q^2}{2}\Big[\frac{q^2}{2}+2g+\frac{4\pi}{3}g_dF_0(q)\Big]}, \quad (6)$$

where

$$F_0(q) = 1 + \tfrac{3}{2}q^2e^{q^2/2}\mathrm{Ei}(-q^2/2), \quad (7)$$

with $\mathrm{Ei}(x)$ being the exponential integral function. Using Eqs. (5) and (6), we arrive at the corresponding Mathieu equation [30]

$$\frac{d^2u}{dt^2} + [\epsilon^2(q) + 2\omega^2b(q,\omega,\alpha)\cos(2\omega t)]u = 0, \quad (8)$$

with

$$b(q,\omega,\alpha) = \frac{2\pi}{3\omega^2}\overline{g}_d\alpha q^2F_0(q). \quad (9)$$

Following the Floquet theorem [31], the solutions of Eq. (8) are of the form $u(t) = e^{\tilde{\sigma}t}f(t)$, where $f(t) = f(t+\pi/\omega)$

and $\tilde{\sigma}(q,\omega,\alpha)$ is the Floquet characteristic exponent, which can be found numerically. If the real part $\sigma \equiv \mathrm{Re}(\tilde{\sigma}) > 0$, the homogeneous quasi-1D BEC becomes dynamically unstable and Faraday patterns emerge. The typical wavelength of the pattern will be determined by the most unstable mode, i.e., that with the largest σ. In the limit of small driving amplitude $\alpha \to 0$, the properties of the pattern are governed by momenta q obeying parametric resonances $n\omega = \epsilon_n(q)$.

Contrary to nondipolar BECs with a monotonic spectrum $\epsilon(q)$, dipolar gases may offer a more complex roton-maxon spectrum [26] (Fig. 1). In consequence of this nonmonotonic character, for a specific range of ω, between the roton and maxon frequencies (ω_r and ω_m, respectively) there are three values $q_1 < q_2 < q_3$ satisfying the resonance condition $\omega = \epsilon(q)$. Figure 2 shows the stability diagram for a driving frequency in this particular window. As expected, for small amplitudes α, the three instability tongues (white regions) correspond exactly to $q_{1,2,3}$ (Fig. 1). This raises an interesting question about which of the three modes dominates the pattern formation. For a 2D geometry, Ref. [27] showed that when modulating dipole-dipole interactions, the most unstable mode corresponds to the intermediate momentum $q_2 < q_r$, with q_r the roton momentum. Crucially, as we show below, this is not the case in a quasi-1D dipolar condensate. This striking contrast between quasi-1D and 2D predictions illustrates once more the key role played by the trapping geometry in dipolar gases.

The problem of the most unstable mode is best understood employing a series expansion of the Floquet exponent with small parameter $b(q,\omega,\alpha)$ [20,32,33], which, for the first parametric resonance $\omega = \epsilon(q)$, yields $\sigma \simeq b(q,\omega,\alpha)/2 \propto q^2 F_0(q)$. Remarkably, in contrast to the 2D case, we find that now the most unstable mode corresponds to the largest momentum $q_3 > q_r$ (solid line in Fig. 2). Figure 3 depicts a momentum of the most unstable mode as a function of the driving frequency ω. The plot confirms that for all

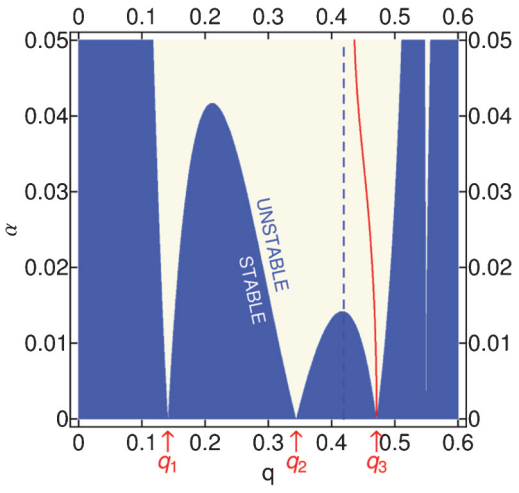

FIG. 2. (Color online) Stability diagram for the parameters of Fig. 1 as a function of the perturbation strength α and momentum q. The unstable region is depicted in white. The red solid line indicates the most unstable mode and the blue dashed line refers to the roton momentum.

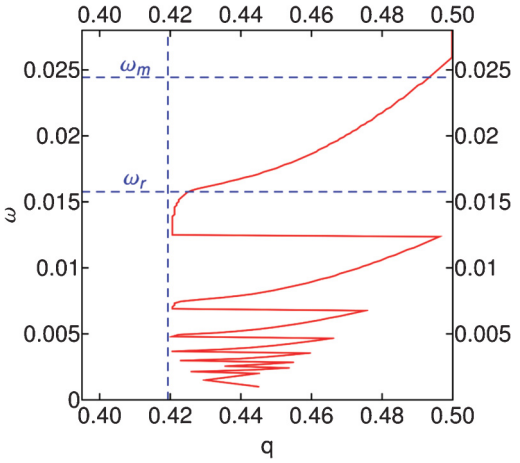

FIG. 3. (Color online) Most unstable momentum q as a function of the driving frequency ω for the parameters of Fig. 1, with $\alpha = 0.01$. The horizontal dashed lines indicate the roton and maxon frequencies ($\omega_{r,m}$) and the vertical line refers to the roton momentum.

frequencies within the window $\omega_m < \omega < \omega_r$, the momentum characterizing the most unstable mode is larger than the roton momentum, contradicting the prediction for a 2D pancake geometry [27]. For $\omega < \omega_r$, alike the 2D case, the observed modulations are dominated by higher resonances with q in the vicinity of q_r. However, unlike the 2D scenario, even in this regime, the most unstable mode in a quasi-1D BEC is characterized by $q > q_r$. We emphasize that the different nature of the Faraday pattern reported here stems solely from the quasi-1D character of the condensate, which leads to a specific momentum dependence of $b(q,\omega,\alpha)$ that differs from that in 2D.

We have simulated numerically the time evolution of the nonlocal nonlinear Schrödinger equation (1) with the parametrically driven nonlinearity, according to Eq. (3). The emergent pattern has been examined by means of Fourier transform of the condensate density, which confirmed the results for the most unstable mode that we obtained within the Mathieu analysis.

IV. FARADAY PATTERNS IN TWO 1D DIPOLAR BOSE-EINSTEIN CONDENSATES

We now turn to the study of Faraday patterns in two parallel quasi-1D dipolar BECs. For nondipolar BECs, in the absence of hopping, each BEC behaves independently, and hence an experiment with two BECs reduces to two uncorrelated experiments with a single condensate. The situation is radically different in dipolar BECs, since, despite the absence of hopping, the nonlocal character of the dipolar potential gives rise to a coupling between the two BECs, with the strength of the intercondensate interactions governed by $F_1(k_z)$. These nonlocal interactions lead to a collective character of the elementary excitations that are shared among the two quasi-1D condensates [28,34]. Consequently, the excitation spectrum

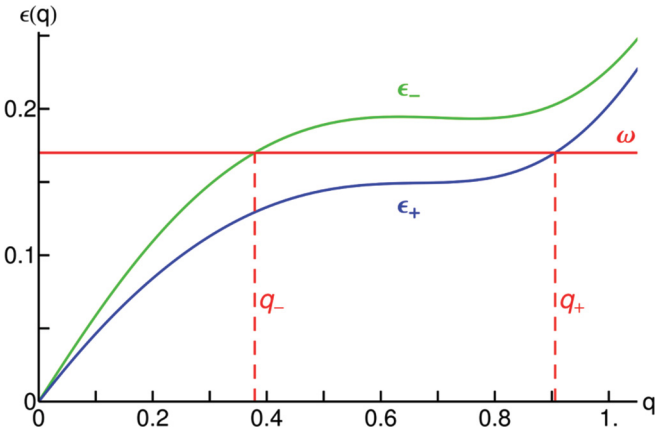

FIG. 4. (Color online) Elementary excitations of two parallel quasi-1D dipolar BECs for $g = -0.0629$, $\overline{g}_d = 0.1749$, and $\Delta/l_\perp = 6$. Note the two branches of the elementary excitations $\epsilon_\pm(q)$, corresponding, respectively, to symmetric and antisymmetric modes with respect to the transposition of traps $j = 1 \leftrightarrow j = 2$.

unfolds into two branches,

$$\epsilon_\pm(q) = \sqrt{\frac{q^2}{2}\left\{\frac{q^2}{2} + 2g + \frac{4\pi}{3}g_d[F_0(q) \pm F_1(q)]\right\}}, \quad (10)$$

which correspond, respectively, to symmetric and antisymmetric states with respect to the transposition of traps $j = 1 \leftrightarrow j = 2$.

Interestingly, this implies that a periodic modulation of the dipolar interactions yields two different parametric resonances for each driving frequency $\omega = \epsilon_\pm(q_\pm)$, even in the absence of the roton minimum (see Fig. 4). Note that the patterns are characterized not only by their momentum $q_\pm$ but also by their symmetric (+) or antisymmetric (−) character. In analogy to Sec. III, the double solution raises a fundamental question about which of these two modes is the most unstable, and hence provides the dominant Faraday pattern. We stress that this nontrivial physics stems directly from the intercondensate interactions, which lead to the splitting between the two branches in the spectrum, being a qualitatively new feature of dipolar condensates.

Similarly to the previous section, we employ Eq. (5) for $j = 1,2$, and the spectra (10). In turn, we obtain two decoupled Mathieu equations for the symmetric and antisymmetric combinations $u_\pm = u_1 \pm u_2$:

$$\frac{d^2u_\pm}{dt^2} + [\epsilon_\pm^2(q) + 2\omega^2 b_\pm(q,\omega,\alpha)\cos(2\omega t)]u = 0, \quad (11)$$

with

$$b_\pm(q,\omega,\alpha) = \frac{2\pi}{3\omega^2}\overline{g}_d\alpha q^2[F_0(q) \pm F_1(q)], \quad (12)$$

to which we apply the Floquet analysis employed in the study of Eq. (8). As in the case of a single BEC, the first parametric resonances $\omega = \epsilon_\pm(q_\pm)$ are characterized by the Floquet exponent $\sigma_\pm \simeq b_\pm(q,\omega,\alpha)/2 \propto q^2[F_0(q) \pm F_1(q)]$, and the emerging Faraday pattern is determined, for each driving frequency separately, by the mode with the largest σ. Remarkably, the involved momentum dependence of $F_0(q) \pm F_1(q)$ leads to an intricate relation between the Floquet exponents and the driving frequency ω, as presented in Fig. 5.

Crucially, the curves $\sigma_\pm(\omega)$ cross at a critical frequency ω_c. In consequence, we expect a distinct transition, as a function of the driving frequency ω, between the symmetric Faraday pattern for $\omega < \omega_c$ and the antisymmetric pattern for $\omega > \omega_c$. Such transition is marked by an abrupt change of the patterns in both condensates from a maximum-maximum alignment (correlated patterns) to a maximum-minimum alignment (anticorrelated patterns), as depicted in the corresponding insets of Figs. 6 and 7. Moreover, for $\omega = \omega_c$, the patterns in both condensates exhibit a pronounced change of the wavelength of the modulation, from $l_+ = 2\pi/q_+(\omega_c)$ to $l_- = 2\pi/q_-(\omega_c)$.

This transition has been confirmed by means of direct numerical simulations of Eq. (1), with the parametric driving governed by Eq. (3). As for a single condensate, we Fourier transform the density of each condensate to obtain the dominant momenta of the emergent Faraday patterns. The results, in the vicinity of the critical frequency ω_c, are depicted in Fig. 6, where, on top of the spectra $\epsilon_\pm$, for each driving frequency ω we indicate with a circle the momentum value where the numerically evaluated $\hat{n}_j(k_z)$ shows a marked maximum. We find that, in agreement with the results for $\sigma_\pm(\omega)$ presented in Fig. 5, for ω well below ω_c the pattern presents a single momentum component at q_+ and it is characterized by a correlation between the patterns in both quasi-1D BECs. In contrast, for ω well above ω_c, a single momentum component at q_- is observed and the patterns in the two quasi-1D BECs are anticorrelated.

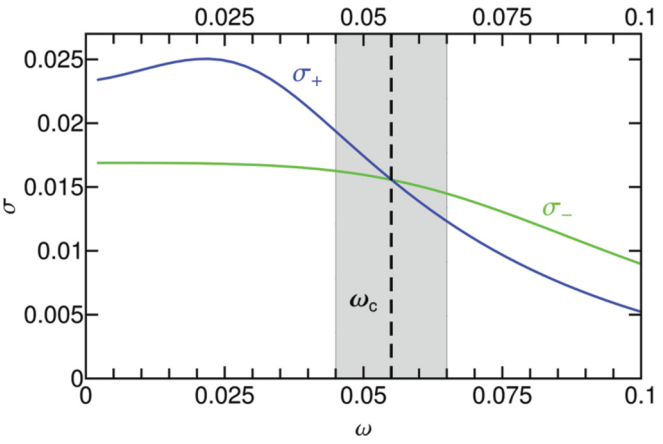

FIG. 5. (Color online) Real part $\sigma_\pm$ of the Floquet exponent, corresponding to the first parametric resonance for the symmetric and antisymmetric excitation branches $\omega = \epsilon_\pm(q)$, as a function of the driving frequency ω. Note that at a critical frequency $\omega_c = 0.055$, both exponents are equal, $\sigma_+ = \sigma_-$, indicating a transition between the symmetric and the antisymmetric Faraday pattern. In the figure, we employ $g = -0.0435$, $\overline{g}_d = 0.0437$, $\Delta = 6l_\perp$, and $\alpha = 0.02$.

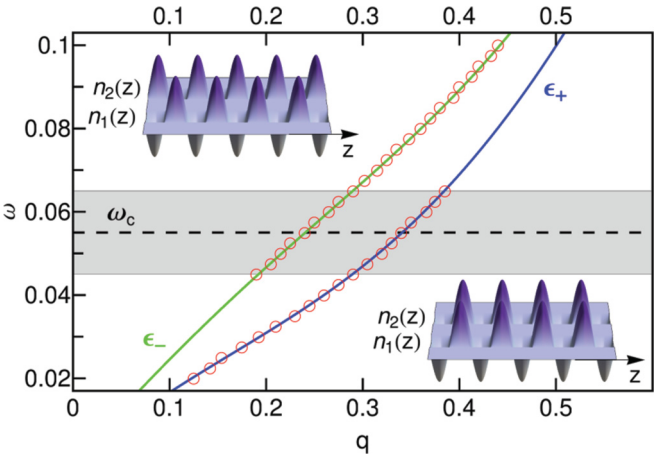

FIG. 6. (Color online) Analysis of the pattern selection as a function of the driving frequency ω, in the neighborhood of the critical frequency ω_c (for the same parameters as in Fig. 5). The solid lines represent the excitation branches. For each ω, we indicate with a circle a momentum value where the numerical Fourier transform $\hat{n}_j(k_z)$ of the Faraday pattern shows a clear maximum. For ω well below (above) ω_c, we observe a single peak at q_+ (q_-), indicating that a symmetric (antisymmetric) Faraday pattern emerges (see insets). In the vicinity of ω_c (shaded region), both modes are equally unstable and we observe the two corresponding peaks occurring simultaneously in the Fourier transform (see text).

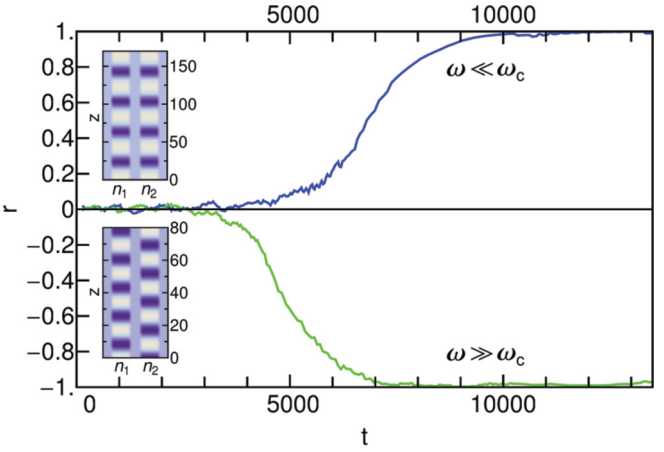

FIG. 7. (Color online) Correlation function $r(t)$ for the same parameters as in Fig. 6 ($\omega_c = 0.055$). The upper curve, which corresponds to $\omega = 0.025 < \omega_c$, approaches $r = 1$ indicating a perfectly correlated pattern in both quasi-1D traps. The lower curve, which corresponds to $\omega = 0.08 > \omega_c$, reaches $r = -1$ proving a perfect anticorrelation between the Faraday patterns in the two traps. The insets show the corresponding numerical results for the density distribution $n_j(z)$ for $t = 11\ 000$, with the bright (dark) colors indicating density maxima (minima). Naturally, for sufficiently long times, well beyond the linear regime, the Faraday patterns and their correlations are eventually destroyed.

In order to quantify the transition between correlated and anticorrelated patterns, we introduce the correlation coefficient

$$r = \frac{\int dz\, S_{n_1}(z) S_{n_2}(z)}{\sqrt{\int dz\, S_{n_1}^2(z)}\sqrt{\int dz\, S_{n_2}^2(z)}}, \tag{13}$$

where $S_{n_j}(z) = n_j(z) - \overline{n_j}$, with $\overline{n_j}$ as the average density in a trap j. The pattern correlation is then characterized by $r > 0$, whereas the anticorrelation leads to $r < 0$. Figure 7 illustrates the radically different time evolution of the correlation coefficient below and above the critical driving ω_c. Clearly, for frequencies sufficiently smaller (larger) than ω_c, the system arrives at a perfectly correlated (anticorrelated) pattern with $r = 1$ ($r = -1$).

An interesting scenario occurs for driving frequencies in the vicinity of the critical ω_c (shaded region in Figs. 5 and 6), where both the symmetric pattern with wavelength l_+ and the antisymmetric pattern with wavelength l_- are equally unstable. In consequence, the Fourier transform of the density in each quasi-1D BEC shows a simultaneous appearance of both momentum peaks, q_+ and q_- (see Fig. 6).

Note that at $\omega = \omega_c$, not only $\epsilon_+(q_+) = \epsilon_-(q_-)$ but also $b_+(q_+,\omega,\alpha) = b_-(q_-,\omega,\alpha)$, and hence the two Mathieu equations (11) for u_+ and u_- become identical. This symmetry is, however, spontaneously broken in experiments due to quantum and thermal fluctuations, which lead to different initial conditions (populations) for both modes that change randomly from one realization to another. This spontaneous symmetry-breaking mechanism is best studied quantitatively by considering the relative weight of the momentum peaks at q_+ and q_- in the Fourier transform of the density $\hat{n}(k_z)$. To this end, we define the imbalance parameter

$$\chi(t) = \frac{\hat{n}(q_+,t) - \hat{n}(q_-,t)}{\hat{n}(q_+,t) + \hat{n}(q_-,t)}. \tag{14}$$

For ω well below or above ω_c, once the pattern emerges, $\chi(t) = \pm 1$. In the vicinity of ω_c, however, the imbalance parameter $\chi(t)$ shows a clear periodicity with frequency 2ω (see Fig. 8). Note that these oscillations do not result from nonlinear competition, as they occur well within the linear regime. In fact, the 2ω oscillations of $\chi(t)$ originate in different,

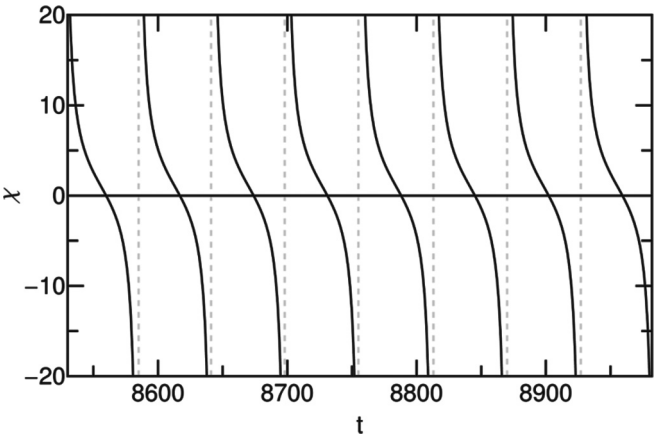

FIG. 8. Population imbalance $\chi(t)$ between the two peaks at $q_\pm(\omega_c)$ for the critical driving $\omega = \omega_c$ (for the same parameters as Fig. 6). Note the 2ω periodicity ($T = \pi/\omega = 57.1$) that stems from a spontaneous symmetry-breaking mechanism (see text).

spontaneously chosen, initial conditions for u_+ and u_- that lead to their different time evolution, which can be well approximated by $u_\pm(t) = [u_\pm^c \cos(\omega t) + u_\pm^s \sin(\omega t)] \exp(\sigma \omega t)$, where $u_\pm^{c/s}$ are the constants determined by the initial conditions. Furthermore, spontaneous symmetry-breaking leads to a different result for the imbalance $\chi(t)$ from one realization to another, which we have confirmed by considering small random differences in the initial conditions for our numerical simulations of Eq. (1).

V. CONCLUSIONS

Faraday patterns in dipolar BECs are crucially dependent on the unique properties of the dipole-dipole interactions. In particular, due to the long-range anisotropic nature of the dipolar interactions, the character of the Faraday patterns depends strongly on the dimensionality of the condensates. We have shown that for periodically modulated dipolar interactions, Faraday patterns in 2D and 1D geometries differ substantially in the presence of a roton minimum in the excitation spectrum. Moreover, for parallel quasi-1D dipolar BECs, the intercondensate interactions lead, even in the absence of hopping, to an excitation spectrum characterized by symmetric and antisymmetric modes. This, in turn, gives rise, at a critical driving frequency, to a marked transition between correlated and anticorrelated Faraday patterns in the two condensates. Interestingly, at this transition point, the Faraday pattern selection stems from a spontaneous symmetry-breaking mechanism.

ACKNOWLEDGMENTS

We acknowledge funding by the German-Israeli Foundation, the Cluster of Excellence QUEST, and the DFG (SA1031/6).

[1] A. Griesmaier, J. Werner, S. Hensler, J. Stuhler, and T. Pfau, Phys. Rev. Lett. **94**, 160401 (2005).
[2] M. Lu, N. Q. Burdick, S. H. Youn, and B. L. Lev, Phys. Rev. Lett. **107**, 190401 (2011).
[3] K. Aikawa, A. Frisch, M. Mark, S. Baier, A. Rietzler, R. Grimm, and F. Ferlaino, Phys. Rev. Lett. **108**, 210401 (2012).
[4] J. Deiglmayr, A. Grochola, M. Repp, K. Mörtlbauer, C. Glück, J. Lange, O. Dulieu, R. Wester, and M. Weidemüller, Phys. Rev. Lett. **101**, 133004 (2008).
[5] K.-K. Ni, S. Ospelkaus, D. Wang, G. Quéméner, B. Neyenhuis, M. H. G. de Miranda, J. L. Bohn, J. Ye, and D. S. Jin, Nature (London) **464**, 1324 (2010).
[6] S. Ospelkaus, K.-K. Ni, G. Quéméner, B. Neyenhuis, D. Wang, M. H. G. de Miranda, J. L. Bohn, J. Ye, and D. S. Jin, Phys. Rev. Lett. **104**, 030402 (2010).
[7] D. Tong, S. M. Farooqi, J. Stanojevic, S. Krishnan, Y. P. Zhang, R. Côté, E. E. Eyler, and P. L. Gould, Phys. Rev. Lett. **93**, 063001 (2004).
[8] M. Baranov, Phys. Rep. **464**, 71 (2008).
[9] T. Lahaye, C. Menotti, L. Santos, M. Lewenstein, and T. Pfau, Rep. Prog. Phys. **72**, 126401 (2009).
[10] M. Fattori, G. Roati, B. Deissler, C. D'Errico, M. Zaccanti, M. Jona-Lasinio, L. Santos, M. Inguscio, and G. Modugno, Phys. Rev. Lett. **101**, 190405 (2008).
[11] S. Müller, J. Billy, E. A. L. Henn, H. Kadau, A. Griesmaier, M. Jona-Lasinio, L. Santos, and T. Pfau, Phys. Rev. A **84**, 053601 (2011).
[12] J. Billy, A. L. Henn, S. Müller, T. Maier, H. Kadau, A. Griesmaier, M. Jona-Lasinio, L. Santos, and T. Pfau, arXiv:1205.5176.
[13] M. Faraday, Philos. Trans. R. Soc. London **121**, 299 (1831).
[14] M. C. Cross and P. C. Hohenberg, Rev. Mod. Phys. **65**, 851 (1993).
[15] D. Binks and W. van de Water, Phys. Rev. Lett. **78**, 4043 (1997).
[16] C. Szwaj, S. Bielawski, D. Derozier, and T. Erneux, Phys. Rev. Lett. **80**, 3968 (1998).
[17] H. Abe, T. Ueda, M. Morikawa, Y. Saitoh, R. Nomura, and Y. Okuda, Phys. Rev. E **76**, 046305 (2007).
[18] K. Staliunas, S. Longhi, and G. J. de Valcárcel, Phys. Rev. Lett. **89**, 210406 (2002).
[19] K. Staliunas, S. Longhi, and G. J. de Valcárcel, Phys. Rev. A **70**, 011601 (2004).
[20] A. I. Nicolin, R. Carretero-González, and P. G. Kevrekidis, Phys. Rev. A **76**, 063609 (2007).
[21] A. I. Nicolin, Phys. Rev. E **84**, 056202 (2011).
[22] A. I. Nicolin, Physica A **391**, 1062 (2012).
[23] A. Balaž and A. I. Nicolin, Phys. Rev. A **85**, 023613 (2012).
[24] P. Engels, C. Atherton, and M. A. Hoefer, Phys. Rev. Lett. **98**, 095301 (2007).
[25] M. Modugno, C. Tozzo, and F. Dalfovo, Phys. Rev. A **74**, 061601 (2006).
[26] L. Santos, G. V. Shlyapnikov, and M. Lewenstein, Phys. Rev. Lett. **90**, 250403 (2003).
[27] R. Nath and L. Santos, Phys. Rev. A **81**, 033626 (2010).
[28] K. Łakomy, R. Nath, and L. Santos, Phys. Rev. A **85**, 033618 (2012).
[29] K. Łakomy, R. Nath, and L. Santos, Phys. Rev. A **86**, 013610 (2012).
[30] N. W. McLachlan, *Theory and Applications of Mathieu Functions* (Clarendon, Oxford, 1947).
[31] P. M. Morse and H. Feshbach, *Methods of Theoretical Physics, Part I* (McGraw-Hill, New York, 1953).
[32] F. Tisserand, *Trait de Mcanique Cleste, Tome III* (Gauthier-Villars, Paris, 1894).
[33] A. I. Nicolin, Ph.D. thesis, The Niels Bohr Institute, Copenhagen, Denmark, 2008.
[34] M. Klawunn and L. Santos, Phys. Rev. A **80**, 013611 (2009).